THEORETICAL EVOLUTION OF A HYDROGEN-HELIUM STAR OF 3 $M_\odot$ FROM THE PRE-MAIN SEQUENCE TO THE CORE HELIUM-EXHAUSTION PHASE

DILHAN EZER

Goddard Institute for Space Studies, NASA, New York, U.S.A.

and

Belfer Graduate School of Science, Yeshiva University, New York, N.Y., U.S.A.

(Received 23 May, 1972)

Abstract. The evolution of a first-generation 3 $M_\odot$ star from the threshold of stability through the stage of helium exhaustion in the core has been studied. The total time elapsed is 4.174×10^8 yr and most of this time is spent in the blue-giant region of the *H-R* diagram. Hydrogen-burning near the Main Sequence occurs at a high central temperature via the proton-proton chain until the triple-alpha reactions generate a small amount of C^{12} toward the end of the hydrogen-burning phase. The corresponding evolution time is longer than that of a normal population I star with the same mass. The ignition of the triple-alpha processes begins in a mildly degenerate, small convective core while the star still has a high surface temperature. Helium-burning in the core, coupled with hydrogen-burning in the shell, occupies a period of about 1.8×10^7 yr, which is only one-third that of a normal star. The mass of the star interior to the hydrogen shell source has increased to a value of 0.50 $M_\odot$ near the end of core helium exhaustion. This region maintains an inhomogeneous composition composed of helium, carbon and oxygen.

1. Introduction

It is generally believed that stars in the mass range of 3.5 $M_\odot$–8 $M_\odot$ undergo supernova explosion and form neutron star remnants or pulsars (Paczynski, 1970; Barkat, 1971; Cameron and Truran, 1971). This range of mass is suggested by stellar evolutionary calculations for population I stars. A star slightly less massive than 3.5 $M_\odot$, say a 3 $M_\odot$ star, lies in the critical region where the final configuration is uncertain. It might form a carbon-oxygen core which is more massive then the carbon-burning mass limit and which is not sufficiently degenerate to cool off during contraction; then, the core heats up until it reaches the temperature of carbon burning. Or, a degenerate core might form, grow in mass, approach the limiting mass for a stable white dwarf, and finally collapse (Biermann and Kippenhahn, 1971).

An earlier evolutionary study of a 3 $M_\odot$ star population I composition was carried out from the main-sequence phase through core helium burning by Iben (1965b) and for later evolutionary phases by Paczynski (1970). If big-bang nucleosynthesis is responsible for the original formation of helium, the first generation of 3 $M_\odot$ stars should contain about 80% hydrogen and 20% helium (Ezer and Cameron, 1971b). Normally, stars of mass greater than about 2 $M_\odot$, burn hydrogen through the CN-cycle on the Main Sequence. In the absence of heavy elements, a first-generation star of 3 $M_\odot$ should convert hydrogen to helium by the proton-proton reactions. There-

Astrophysics and Space Science **18** (1972) 226–245.

fore, its structural characteristics and evolution on the main sequence, and subsequent phases of evolution, are expected to be different from those of a normal star. The complete evolutionary history of such a star will be important for studies of the chemical evolution of the Galaxy (Truran and Cameron, 1971).

The present study was undertaken to follow the evolution of a first-generation 3 $M_\odot$ star from the threshold of stability through the final stages of its evolution. In this paper, the results of the evolutionary study up to the core helium-exhaustion phase will be presented. The subsequent evolution will be examined in another paper.

2. Outline of the Procedure

The present evolutionary study was carried out by the use of the Henyey method. The evolutionary program used previously (Ezer and Cameron, 1971b) has been extended to take account of the changes during the late phases of evolution.

Two different sets of opacity tables were used. The first set was for three hydrogen-helium mixtures, in which the hydrogen-helium ratio was 4, 1, and 0. The second set was for the helium-carbon-oxygen mixture required during the late stages of evolution: the ratio of helium to carbon-oxygen was varied from 1.2 to 0, with the last mixture containing equal amounts of carbon and oxygen. These opacities were obtained from the Cox opacity code made available to the Institute for Space Studies.

The energy sources were: gravitational contraction, the proton-proton chain, the CN cycle, and the helium-burning reactions. The nuclear parameters and physical assumptions for the hydrogen burning reactions were the same as in the work of Ezer and Cameron (1971a).

Helium burning reactions were: the triple-alpha reaction, $C^{12}(\alpha, \gamma)O^{16}$, $N^{14}(\alpha, \gamma)F^{18}$, and $O^{18}(\alpha, \gamma)Ne^{22}$ reactions. Nuclear parameters for these reactions were adopted from the review by Fowler *et al.* (1967). But the rate of the triple-alpha reaction quoted by Fowler *et al.* (1967) was corrected by a factor of $\exp(-0.138/T_9)$ due to the recent remeasurement of the excitation energy of the second excited state of C^{12} (Austin *et al.*, 1971). The cross-section constant for the $N^{14}(\alpha, \gamma)F^{18}$ reaction was taken to be $S = 1.5 \times 10^6$ keV-b (Parker 1968), which is larger than the revised value given by Cauch *et al.* (1972).

Energy losses by photo-neutrinos and plasma neutrinos were included throughout the evolutionary study. The rate of neutrino emission was calculated with formulae given by Beaudet *et al.* (1967).

The electron screening factors for the thermonuclear reactions were obtained following Reeves' (1965) evaluation of the work of Salpeter (1954).

Changes in the abundances of H^1, He^4, C^{12}, N^{14}, O^{16}, O^{18}, and Ne^{22} were followed explicitly.

Turbulent motions of convecting elements in the interior of the star were treated by the Böhm-Vitense (1958) mixing-length theory, and the ratio of mixing-length to pressure scale height, $1/H$, was taken to be 1.3.

The rest of the imput physics was the same as that used in Ezer and Cameron (1971b).

3. Over-all Results

The theoretical evolutionary track in the *H-R* diagram of the H-He star of 3 $M_\odot$, from the threshold of stability up to helium exhaustion in the core, is shown in Figure 1. The properties of the models at the points indicated by the capital letters along the track are explained in what follows. The characteristics of some selected evolutionary models are summarized in Table I. The first column gives the age of the models in

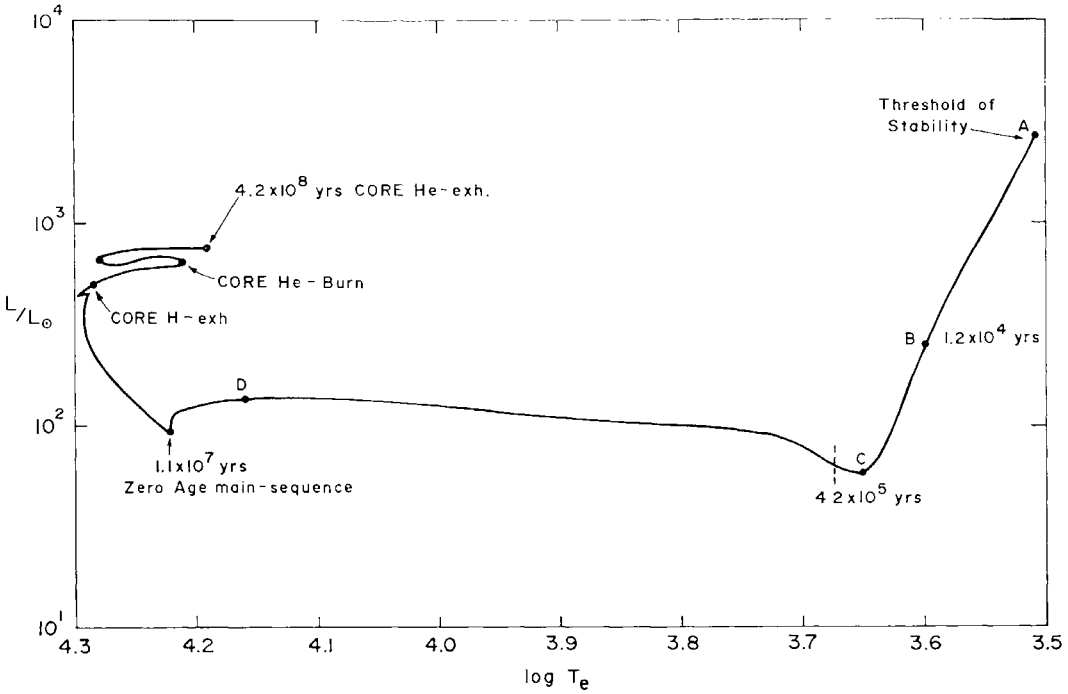

Fig. 1. The theoretical Hertzsprung-Russell diagram for the H-He star of 3 $M_\odot$.

years. The second column indicates the position of the star in the *H-R* diagram. The columns from three to eight give, in turn: the radius and luminosity of the models in solar units; the logarithm of effective temperature, T_e; the central temperature, T_c; the density, ϱ_c; and the mass fraction inside the convective core. Columns nine, ten, eleven and twelve list the abundances of hydrogen, helium, carbon, and oxygen, by mass, at the center of the star. The last column gives the mass fraction of the hydrogen-exhausted core.

The variation of the central values of temperature and density is displayed in Figure 2. The temperature and density combinations at which the major events occur during the evolution are also marked in the figure. The degree of electron degeneracy in the core increases slightly after the core hydrogen-burning phase; nevertheless, throughout the evolution under study, the core reached only moderate degeneracy.

In Figure 3, the evolutionary track in the *H-R* diagram of the H-He star of $3M_\odot$ from the zero-age main-sequence through the core helium-exhaustion phase is com-

TABLE I

Characteristics of evolutionary models from the pre-main sequence to the end of core helium burning

Time yr.	Point	$R/R_\odot$	$L/L_\odot$	$\log T_e$	T_c K	ϱ_c gm cm^{-3}	$(M_r/M)_{\text{conc.}}$	X_1	X_4	X_{12}	X_{16}	$(M_r/M)_{x_1}$
0.00	A	1.63×10^2	2.69×10^3	3.51	1.36×10^5	7.35×10^{-6}	1.00	0.800	0.200			
1.24×10^4	B	3.42×10^1	2.53×10^2	3.60	6.36×10^5	7.12×10^{-4}	1.00	0.800	0.200			
2.21×10^5	C	1.26×10^1	5.69×10^1	3.65	1.96×10^6	3.87×10^{-2}	0.23	0.800	0.200			
2.03×10^6	D	1.89×10^0	1.36×10^2	4.16	1.92×10^7	3.83×10^1	0.00	0.800	0.200			
1.10×10^7	a	1.15	9.10×10^1	4.22	2.92×10^7	8.58×10^1	0.10	0.789	0.211			
2.46×10^8	a′	1.30	1.70×10^2	4.26	3.95×10^7	3.15×10^2	0.00	0.220	0.780			
3.82×18^8	b	1.90	4.56×10^2	4.29	8.03×10^7	4.84×10^3	0.00	0.014	0.098	4.71×10^{-11}		
3.86×10^8	c	1.78	4.33	4.30	8.51×10^7	2.14×10^3	0.04	0.015	0.985	5.50×10^{-10}		
3.88×10^8	c′	2.02	4.91	4.28	8.37×10^7	7.14×10^3	0.00	0.000	1.000	1.82×10^{-9}	3.07×10^{-15}	0.04
3.98×10^8	d	2.78	5.96	4.24	9.42×10^7	2.74×10^4	0.00	0.000	1.000	4.92×10^{-5}	1.45×10^{-8}	0.120
3.992×10^8		3.10	6.14	4.22	1.03×10^8	3.39×10^4	0.00		0.999	8.39×10^{-4}	6.73×10^{-7}	0.135
3.995×10^8	e	3.22	6.64	4.21	1.27	1.28×10^4	0.06		0.993	9.73×10^{-3}	1.13×10^{-5}	0.136
3.996×10^8		3.04	6.89	4.23	1.26	1.05×10^4	0.05		0.988	1.48×10^{-2}	2.70×10^{-5}	0.138
4.097×10^8	f	3.29	6.57	4.28	1.38	7.10×10^3	0.06		0.600	0.367	0.033	0.145
4.131×10^8		2.43	6.71	4.28	1.44	7.19×10^3	0.07		0.400	0.510	0.090	0.149
4.174×10^8	g	3.76	7.61	4.20	1.81	2.45×10^4	0.03		0.004	0.596	0.400	0.168

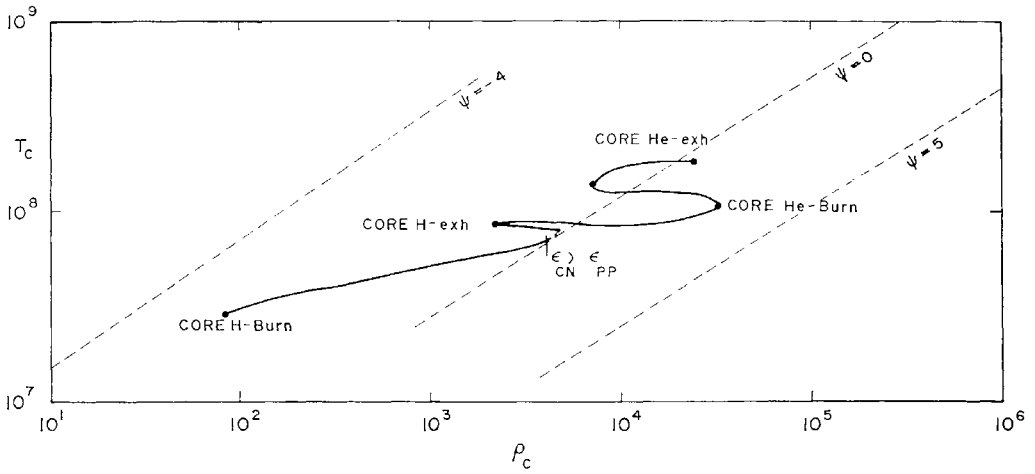

Fig. 2. The central temperature-density diagram for the H-He star of 3 $M_\odot$, covering the whole evolutionary track.

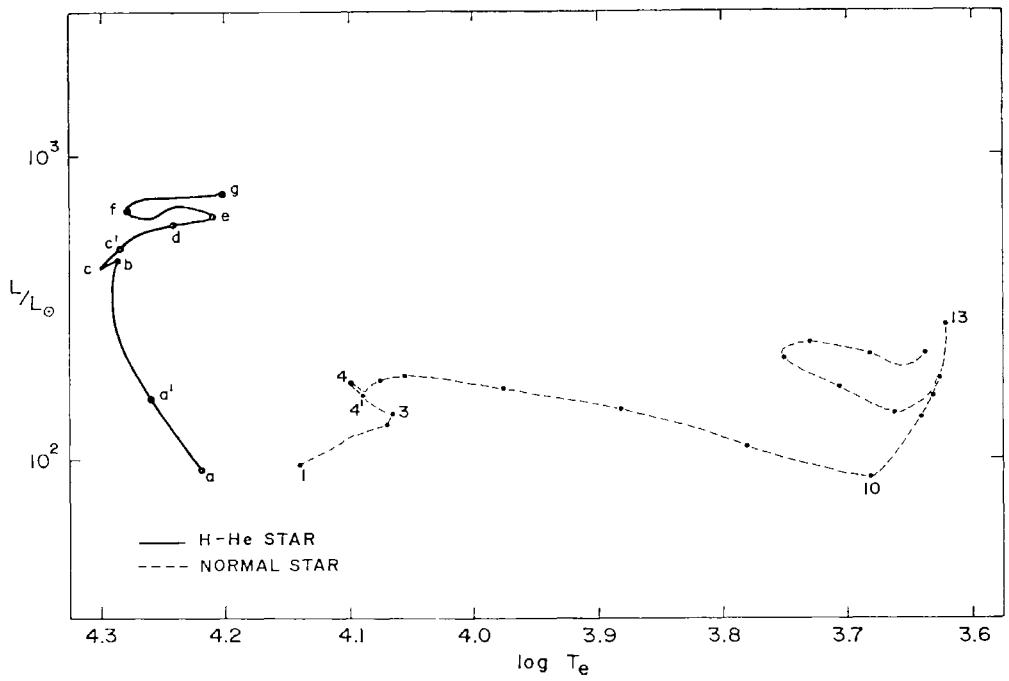

Fig. 3. Comparison of the evolutionary track of the H-He star of 3 $M_\odot$ with that of a normal star of similar mass, in the *H-R* diagram.

pared with that of a normal population I star with the same mass (Iben, 1965). Comparing these two tracks, one can see that, the H-He star of $3M_\odot$ spends most of its life during the phases under consideration in the blue-giant region of the *H-R* diagram.

The lifetimes required by the H-He star of 3 $M_\odot$ and by a normal star to reach different evolutionary phases are summarized in Table II.

The zero-age Main-Sequence and total evolution time of the H-He star of 3 $M_\odot$ are longer than those of a normal star having the same mass. However, the lifetime be-

TABLE II
Evolutionary lifetimes

Evolutionary phase	Lifetimes in years	
	H-He star	Normal star
Zero-age Main-Sequence	1.099×10^7	2.46×10^6
Core hydrogen-exhaustion	3.880×10^8	2.24×10^8
Core helium-burning	3.995×10^8	2.53×10^8
Core helium-exhaustion	4.174×10^8	3.26×10^8

tween the core hydrogen-exhaustion and core helium-exhaustion phases is only one-third of that of a normal star.

4. Pre-Main Sequence Phase

When the H-He star of 3 $M_\odot$ contracts to a radius of 163 $R_\odot$ with a luminosity of 2.7×10^3 $L_\odot$, the condition for energy stability (Ezer and Cameron, 1965, 1967, 1971a) is satisfied. The initial model (corresponding to 'zero' evolution time at the threshold of stability) is fully convective. A radiative core starts to develop when the central temperature and density have risen to 8.04×10^5 K and 1.46×10^{-3} gm cm^{-3}, respectively. The luminosity keeps decreasing until the radiative core extends to about 77% of the stellar mass. After 4.2×10^5 yr of evolution, the convective region of the star has receded practically to surface layers and only covers about 1% of the stellar mass.

Approach to the Main Sequence is not marked by the features which are normally observed in the evolution of a normal star with the same mass (Iben, 1965a; Ezer and Cameron, 1967). In the absence of any heavy elements in the initial composition, the contraction continues until the gravitational source of energy is replaced by nuclear energy from the proton-proton chain reactions.

In Table I, model A is the initial model at the threshold of stability and model B is the last fully convective model. Model C corresponds to the point at which the luminosity drops to its minimum value, and model D is the last purely gravitationally contracting model. The position of the points A, B, C, and D in the *H-R* diagram are indicated in Figure 1.

The H-He star of 3 $M_\odot$ contracts to a radius of 1.5 $R_\odot$, with a luminosity of 1.3×10^2 $L_\odot$, in 2.5 $\times$ 10^6 yr. The central temperature and density attain values of 20×10^6 K and 50 gm/cm^{-3}, respectively, and the rate of energy generation by the p-p chain reactions becomes comparable to that due to gravitational contraction at the center of the star. This slow down the rate of contraction, first near the center and then farther out from the center, More sensitive temperature dependence of the p-p chain reactions causes the formation of a small convective core at the center; this reduces slightly the total energy output of the star. The H-He star of 3 $M_\odot$ reaches the zero-age Main-Sequence in 1.1×10^7 yr with a radius of 1.15 $R_\odot$, which

is 34% smaller than that of a normal star with the same mass. Hence, the corresponding effective temperature of the H-He star is higher. However, the convective core is smaller because the temperature dependence of the proton-proton chain is milder than that of the CN-cycle.

5. Hydrogen-Burning and Hydrogen-Exhaustion Phases

In Figure 3, the position of the zero-age main sequence for the H-He star of 3 $M_\odot$ in the *H-R* diagram is at point a. The physical characteristics of the models during the hydrogen-burning and hydrogen-exhaustion phases (points a–d) are given in Table I.

The zero-age Main-Sequence model is the model in which nuclear burning has just started to lower the initial value of the central hydrogen abundance. The convective core reaches its maximum extent, here equal to 10% of the star's mass. The size of this convective core is about half that in a normal star with the same mass which derives its energy by the CN-cycle reactions. In the evolution of a H-He star, this nuclear burning is entirely due to the p-p chain reactions. But it only supplies a small percentage of the total energy output of the star, since the matter inside the fractional mass 0.56 is still contracting.

The central convective core disappears in 1.39×10^8 yr when the star has a radius of 1.22 $R_\odot$ and a luminosity of 1.19×10^2 $L_\odot$. The unburned central hydrogen content is about 0.496. In contrast to the evolution of a normal star of 3 $M_\odot$, further hydrogen depletion occurs in a partially degenerate, radiative core, and the evolutionary track moves up the main sequence as explained in Ezer and Cameron (1971b). When central hydrogen content has dropped to 0.220 (point a′ in Figure 3), the central temperature and density have risen to 3.95×10^7 K and 3.15×10^2 gm m^{-3}, respectively. The maximum rate of energy generation by the p-p chain reactions has shifted away from the center to mass fraction 0.02.

During the last part of the main hydrogen-burning phase, hydrogen depletion occurs over a large fraction of the stellar mass. The star does not suffer an over-all contraction as in the case of normal stars. As the central regions contract slowly, the surface layers expand slightly, while the luminosity keeps rising with the increasing molecular weight. The evolutionary path proceeds along the main sequence, as shown in Figure 3, until the hydrogen content at the center has dropped to 0.014 (point b). By that time, the central temperature and density have risen to 8.03×10^7 K and 4.84×10^3 gm cm^{-3}, respectively. The fractional amount of carbon formed by the triple-alpha reactions at the center is 4.71×10^{-11}. The continued operation of the triple-alpha reactions makes the contribution to the energy generation from the CN-cycle reactions larger than that of the p-p chain reactions at the center. In Figure 4, the distributions of the energy generation by the p-p chain reactions (ε_{pp}), and by the CN-cycle reactions (ε_{CN}), are given as a function of stellar mass fraction at point b. The scaling factor is 1.17×10^3 erg gm^{-1} s^{-1}. The variation with mass fraction of temperature (T/T_c), density (ϱ/ϱ_c), luminosity (L/L_T), radius (R/R_T) and hydrogen abundance (X_1) by mass are also plotted in Figure 4. A

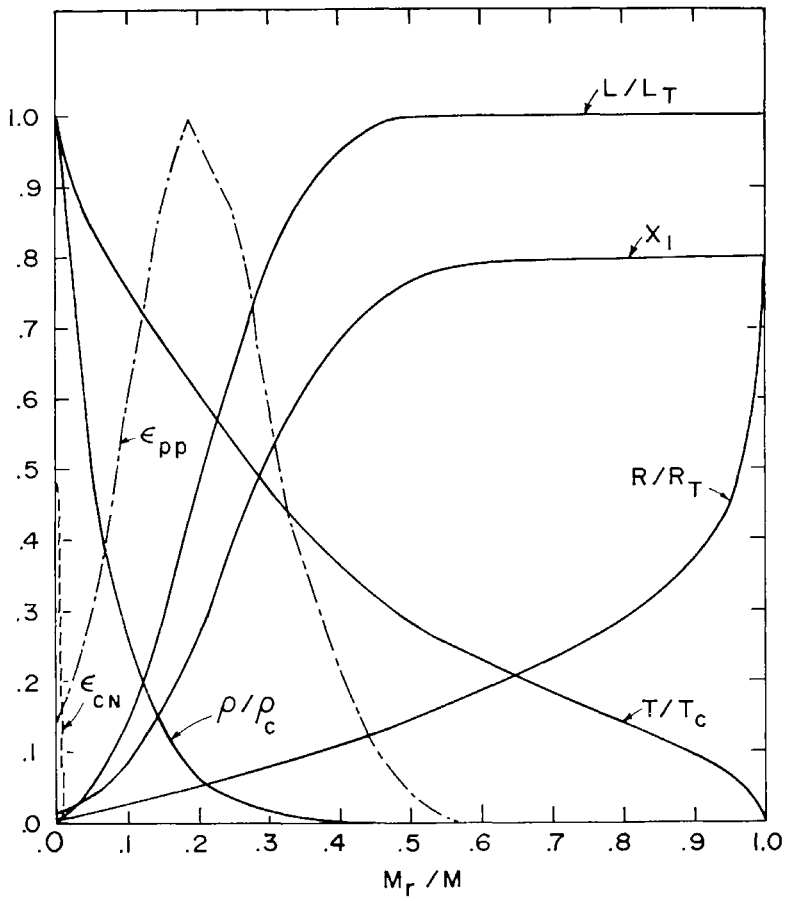

Fig. 4. The variation with mass fraction of temperature (T/T_c), density (ϱ/ϱ_c), luminosity (L/L_T), radius (R/R_T), H-abundance by mass (X_1), energy generation rate by the p-p chain reactions (ε_{pp}), and by the CN-cycle reaction (ε_{CN}), at $t = 3.82 \times 10^8$ yr. The scaling factor for the energy generation rates is 1.17×10^3 erg gm^{-1} s^{-1}.

large rate of energy generation by the CN-cycle reactions of the center of the star causes the rapid development of a convective core, which covers about 4% of the stellar mass. While the partially degenerate central regions of the star are expanding, the central density decreases (see Figure 2), the luminosity declines, the total radius of the star shrinks in order to balance the energy outflow, and the star moves along the track to point c.

During the main phase of hydrogen burning in a normal star of 3 $M_\odot$ as hydrogen in the convective core is depleted by the CN-cycle reactions, the energy balance in the star is maintained by core contraction and envelope expansion, and the star moves from point 1 to 3. With further reduction of hydrogen, the star suffers an overall contraction and moves from point 3 to 4. Now the major nuclear burning region moves away from the center to the regions containing unburned hydrogen. Hydrogen burning in the developing shell causes expansion of the outside layers and, therefore the luminosity drops slightly (point 4′).

In the evolution of the 3 $M_\odot$ H-He star, rapid contraction of the core following exhaustion of hydrogen in the central conventive region brings the star to point c′ on the evolutionary track. Meanwhile the central temperature decreases slightly, and the central density and degree of electron degeneracy increases. At this time, nuclear energy production occurs only outside the fractional mass 0.04. Due to the high temperatures prevailing inside the star, the hydrogen-burning shell is fairly thick. The rate of energy generation from the CN-cycle reactions reaches its maximum value at mass fraction 0.045 where the fractional carbon abundance is 5.3×10^{-10}. The less temperature-sensitive p-p chain reactions attain their maximum rate of energy production at mass fraction 0.20. The inner 25% of the stellar mass undergoes gravitational contraction, and the energy generation due to this contraction is 2.5×10^2 erg gm^{-1} s^{-1} at the center of the star. The resulting flux produces a small temperature gradient in the core, $\log T_c/T_r < 0.05$, where T_r is the temperature

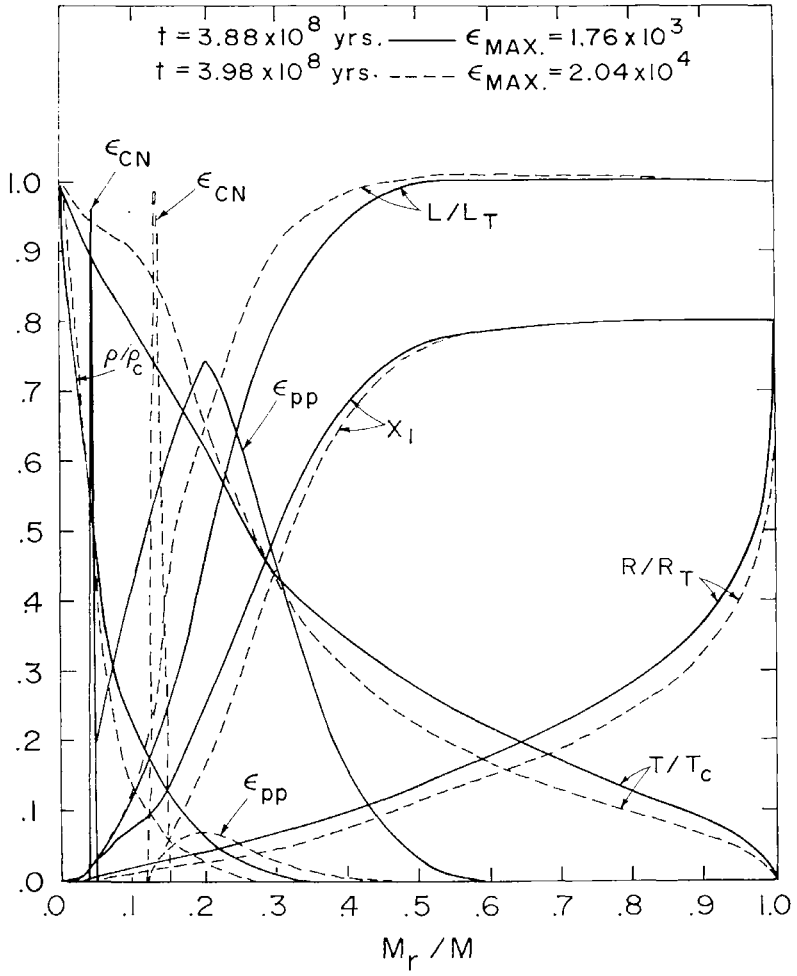

Fig. 5a. The variation with mass fraction of the variables defined under Figure 4 at $t = 3.88 \times 10^8$ yr, corresponding to the model that follows the one in which the convective core disappears (solid lines); and at $t = 3.98 \times 10^8$ yr for a later model in which the hydrogen-exhausted core covers about 12% of the stellar mass (dashed lines). The scaling factors for the energy generation rates are given in the figure.

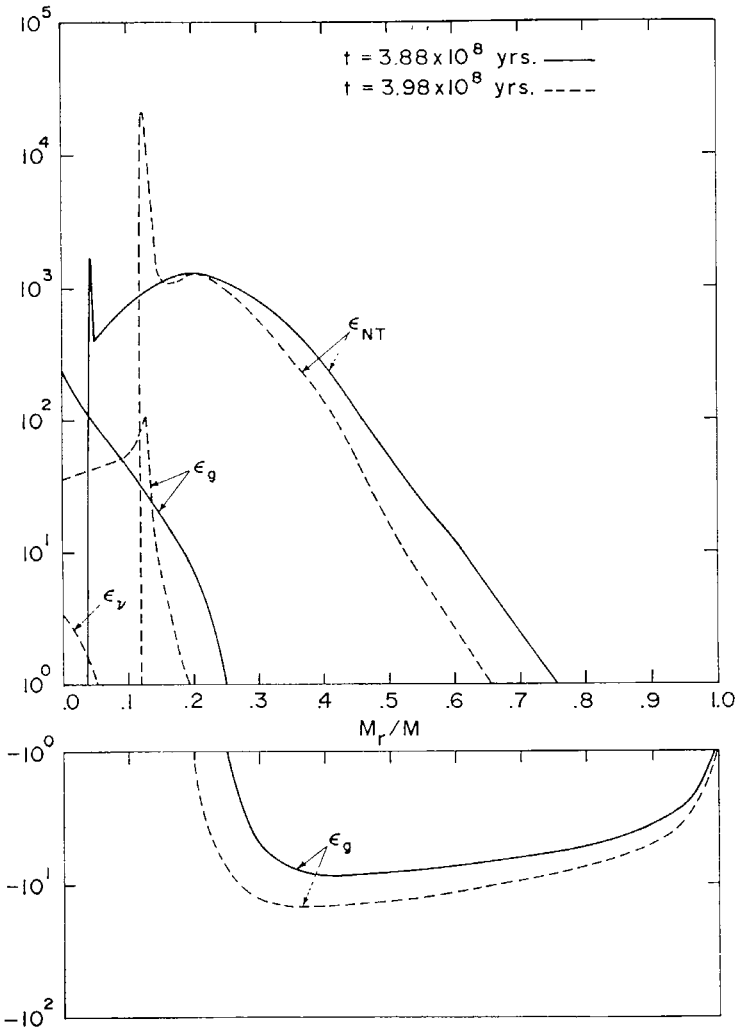

Fig. 5b. The variation with mass fraction of the rate of energy generation from all nuclear burning (ε_{NT}), from gravitational contraction (ε_g), and from neutrino processes (ε_ν) for the models corresponding to those of Figure 5a. When ε_g is negative, it is plotted in the lower part of the figure.

at the boundary of the core. The star is very centrally condensed; about 97% of the star's mass lies within half the radius of the star. In Figure 5a, the rate of energy generation by the p-p chain reactions (ε_{pp}) and by the CN-cycle reactions (ε_{CN}), the hydrogen abundance by mass (X_1), the distribution of temperature (T/T_c), density (ϱ/ϱ_c), luminosity (L/L_T) as a function of mass fraction are shown for the model that immediately follows the one in which the convective core disappears; the solid lines in the figure refer to this model. The same quantities are also plotted in figure 5 a for a later model in which the hydrogen-exhausted core has extended to about 12% of the stellar mass (dashed lines). In Figure 5b, the value of the logarithm of the rate of energy generation from all nuclear burning (ε_{NT}), from the gravitational contraction (ε_g), and from the neutrino processes (ε_ν) are plotted against mass fraction for the models corresponding to those of Figure 5 a, using the same notations.

In about 10^7 yr, the hydrogen-exhausted core has extended to about 12% of the stellar mass. A temperature of 9.42×10^7 K and a density of 2.74×10^4 gm cm^{-3} are reached at the center, and energy generation by the triple-alpha reactions is now important. The fractional carbon abundance at the center is 4.92×10^{-5}, and a sufficient amount of carbon has been formed up to mass fraction 0.15 to broaden the energy-producing shell that is burning via the CN-cycle reactions. About 50% of the total luminosity is produced in a shell between mass fractions 0.120 and 0.145 by the CN-cycle reactions. Hydrogen-burning by the p-p chain reactions occurs in a shell lying between mass fractions 0.14 and 0.65, with a peak value around mass fraction 0.20; here 51% of the total luminosity is produced. The expanding envelope absorbs energy equal to about 1% of the total luminosity. While hydrogen is rapidly consumed by the CN-cycle reactions around mass fraction 0.135, expansion occurs just outside this region. With the node occurring in the vicinity of maximum hydrogen burning, core contraction is accompanied by rapid envelope expansion, persisting all the way to the surface (see Figure 5b). Meanwhile, the high temperatures and densities prevailing deep inside the star make the energy losses from plasma and photon neutrinos become pronounced during the late shell hydrogen-burning stages of the evolution. This affects the increase of the temperature and luminosity in the core of the star. The logarithm of the temperature gradient at mass fraction 0.05 is 0.03, which is smaller than the value right after the beginning of the shell hydrogen-burning phase. Throughout this period of the evolution, the luminosity rises, since the nuclear energy production in the shell increases as (a) the fractional amount of carbon formed by the 3-α reactions increases and (b) matter in the shell becomes hotter and denser, being spatially closer to the center of the star. The expansion of the envelope, accompanied by the decreasing temperature in the outer part of the star, causes the outer edge of the nuclear energy producing shell to move inward in time. As hydrogen is rapidly exhausted at the inner edge of the shell where the temperature is continually rising, the mass contained in the shell decreases; hydrogen burning occurs between mass fraction 0.12 and 0.65 at point d.

6. Core Helium-Burning Phase

From the beginning of the shell hydrogen-burning phase at point c′ up to the point where the hydrogen content is exhausted in the inner 13.5% of the stellar mass at an evolution time of 3.992×10^8 yr, the luminosity and radius of the star have only increased by about one solar unit. The effective temperature of the star 1.64×10^4 K, and the star is located in the blue-giant region of the *H-R* diagram. This is contrary to the situation of a normal star of 3 $M_\odot$, which during that period moves from point 4′ to 10 in its track.

The central temperature and density of the H-He star has now risen to 1.03×10^8 K and 3.39×10^4 gm cm^{-3}. These are high enough to make the energy generation by the triple-alpha reactions contribute to the total nuclear energy generation of the star. The contribution from the triple-alpha reactions is 2.35×10^2 erg gm^{-1} s^{-1} at the

center. The $C^{12}(\alpha, \gamma)O^{16}$ reaction is also operative at the center, but the rate of energy generation by this reaction is only 0.08% of that of the triple-alpha reactions. The ignition of the triple-alpha reactions leads to a slight envelope expansion to balance energy production and energy outflow. Meanwhile the sensitive temperature and density dependences of the triple-alpha reactions cause the development of a convective core, which covers 6% of the stellar mass at 3.995×10^8 yr, corresponding to point e in Figure 3.

The characteristics of the core helium-burning models are also summarized in Table I. The distributions of state and composition variables within the star at point e are shown in Figure 6a. The distributions of energy sources as a function of mass fraction are presented in Figure 6b.

The ignition of the triple-alpha reactions begins in a mildly degenerate, small convective core ($M_c = 0.05\ M_T$) while the star still has high surface temperature. This situation is entirely different from that of a normal star with the same mass, in which helium burning starts in a larger convective core when the star reaches the tip of the red-giant branch in the evolutionary track (point 13).

After the ignition of helium in the core, the luminosity at first slightly increases,

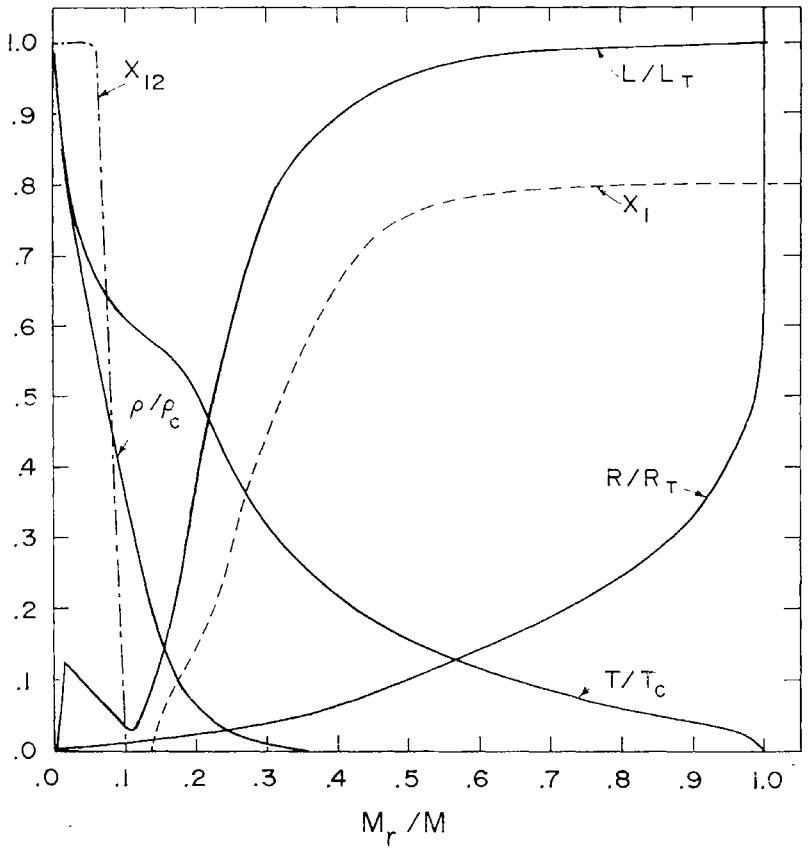

Fig. 6a. The variation with mass fraction of state and composition variables at $t = 3.995 \times 10^8$ yr. X_{12} is the abundance of carbon by mass, and other variables have the same definitions as in Figure 4. The scaling factor for X_{12} is 9.73×10^{-3}.

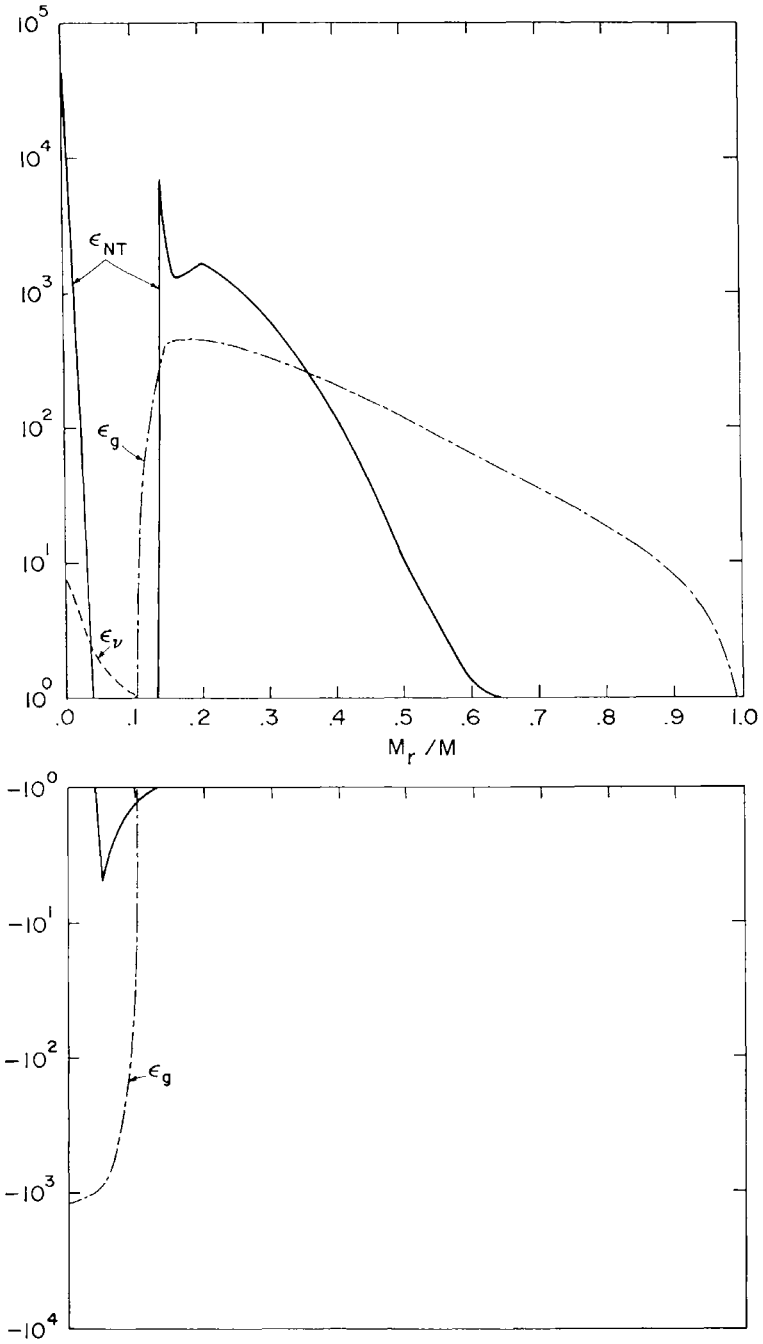

Fig. 6b. The variation with mass fraction of the energy sources defined under Figure 5b for the model corresponding to $t = 3.995 \times 10^8$ yr.

partially as a result of the increase of temperature in the hydrogen-burning shell. But in 10^5 yr, the drop in central density affects the core nuclear burning and the luminosity shows a decline, accompanied by envelope contraction (between points e and f).

At an evolution time of 4.097×10^8 yr the central helium content has been reduced

to 0.60 in the convective core. A temperature of 1.38×10^8 K and a density of 7.10×10^3 gm cm^{-3} are then attained at the center of the star. The fractional carbon abundance has reached 0.337 and energy generation by the $C^{12}(\alpha, \gamma)O^{16}$ reaction becomes important. The total amount of nuclear burning at the center of the star is 4.2×10^4 erg gm^{-1}s^{-1}, 0.5% of this is due to the $C^{12}(\alpha, \gamma)O^{16}$ reaction. Shell hydrogen-burning occurs between mass fractions 0.145 and 0.75. As the inner boundary of the hydrogen-burning shell moves toward larger mass fractions, the rate of energy generation by the CN-cycle decreases with the reduction of carbon formed at the larger mass fractions. The distributions of state and composition variables within the star at $t = 4.097 \times$ $\times 10^8$ yr are given in Figure 7a. The distributions of the energy generation rates are shown in Figures 7b and 7c. The rate of energy generation by the p-p chain reactions has its maximum value at mass fraction 0.26. The acceleration of the material around the layer of maximum hydrogen burning has decreased. But the layers between the core and shell source are rapidly contracting and hence keeping the luminosity almost constant in spite of the increasing rate of energy loss due to neutrino processes.

At 4.131×10^8 yr, the central convective core reaches its maximum size (7% of the stellar mass) when the central helium content had dropped to 0.40. The abundance

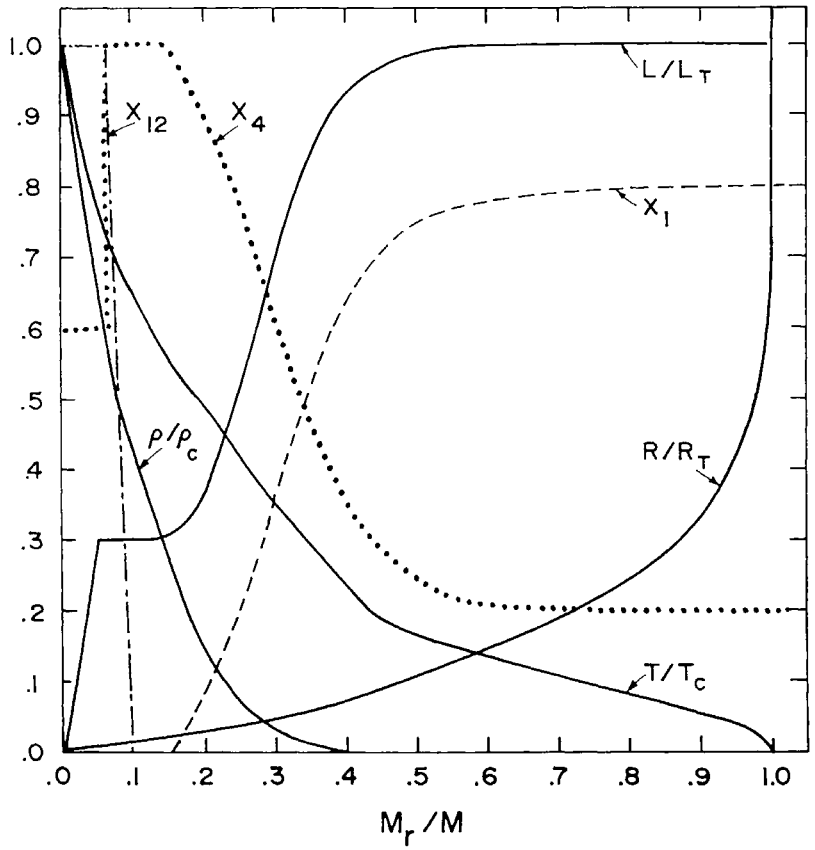

Fig. 7a. The variation with mass fraction of state and composition variables at $t = 4.097 \times 10^8$ yr. X_4 is the abundance of helium by mass, and other variables have the same definitions as in Figures 4 and 6a. The scaling factor for X_{12} is 0.367.

of carbon exceeds that of helium at the center of the star. Central helium is practically exhausted at $t = 4.174 \times 10^8$ y, when the convective core has receded to mass fraction 0,03.

Between $t = 4.131 \times 10^8$ y and $t = 4.178 \times 10^8$ yr, the relation between observable surface variables and core structure is somewhat similar to that obtaining during the core hydrogen-burning phase in the evolution of normal stars. Stellar luminosity and radius increase as the central temperature and density rise.

The distribution of physical and compositional parameters as a function of mass fraction are given in Table IIIa and Table IIIb, for a model corresponding closely to the end of the helium-exhaustion phase. In Table IIIa, the first column gives the fractional mass of the star. The other columns given in turn, the radius (cm), luminosity (erg s^{-1}), temperature (K), and density (gm cm^{-3}), at the selected mass fractions; X_1, X_4, X_{12}, X_{16} are the abundances, by mass, of hydrogen, helium, carbon and oxygen. The last column indicates the mode of energy transfer. In Table IIIb, the columns from two to five give the energy generation rate (erg gm^{-1} s^{-1}), by the different indicated nuclear reactions; the other columns refer to the rates of: neutrino emission, all nuclear reactions, and gravitational contraction. They are listed for the same mass fractions as given in Table IIIa. The composition profile inside the star is also pre-

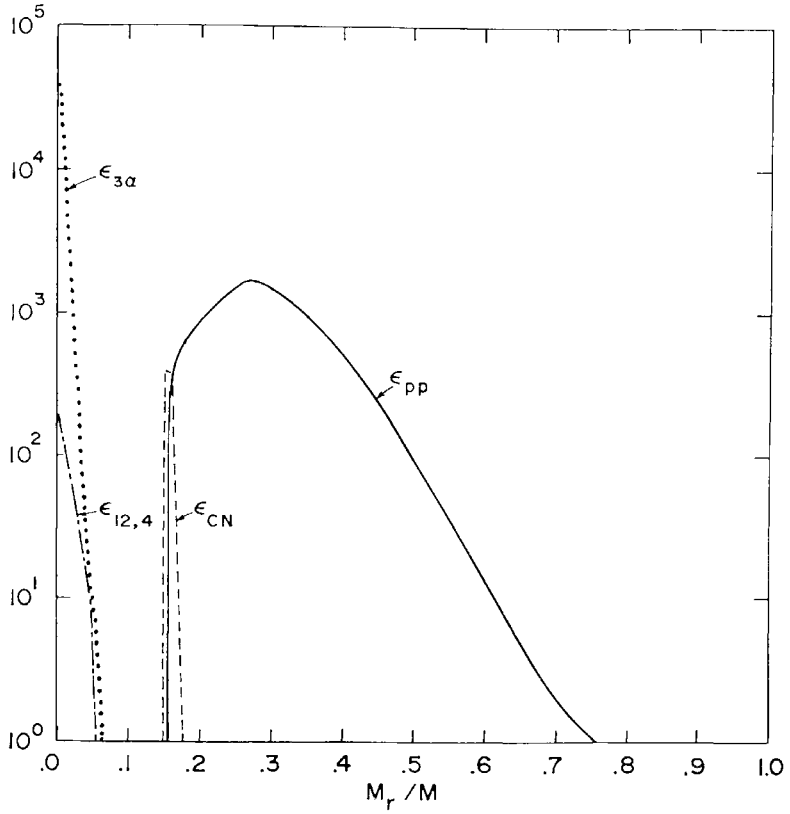

Fig. 7b. The variation with mass fraction of the energy generation rates from the p-p chain reaction (ε_{pp}), from the CN-cycle reactions (ε_{CN}), from the triple-alpha reactions ($\varepsilon_{3\alpha}$), and from the $C^{12}(\alpha, \gamma)\, O^{16}$ reaction, at $t = 4.097 \times 10^8$ yr.

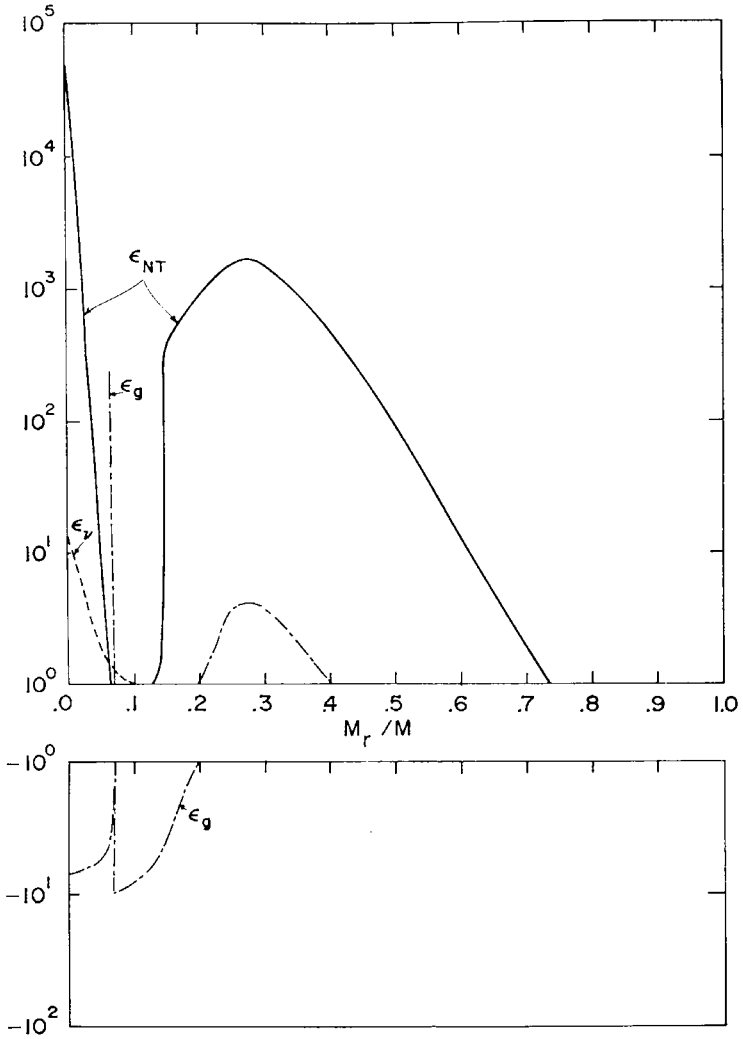

Fig. 7c. The variation with mass fraction of the quantities defined under Figure 5b at $t = 4.097 \times 10^8$ yr.

sented in Figure 8. From the inspection of Tables IIIa, b and Figure 8, it is seen that, near the end of the core helium-exhaustion phase, the convective core of the star has receded to mass fraction 0.03. With the complete exhaustion of helium, the convective core will have entirely disappeared, leaving the star in radiative equilibrium throughout. The fractional abundances of helium, carbon, and oxygen inside the convective core are 0.004, 0.596, and 0.400, respectively. Outside the convective core, up to mass fraction 0.076, a substantial amount of carbon exists partly due to the current operation of the triple-alpha reactions and partly due to the earlier distribution of elements inside the convective core, which once extended up to mass fraction 0.07 during the early core helium-burning phase. In these regions, helium burning mostly proceeds via the $C^{12}(\alpha, \gamma) O^{16}$ reaction.

The main phase of core helium burning, coupled with shell hydrogen burning (points from e to g), occupies about 1.8×10^7 yr. This time is shorter than that of a normal

TABLE IIIA

Characteristics of the model at the end of core helium-exhaustion

$t = 4.174 \times 10^8$ yr

$R = 3.76\ R_\odot$, $L = 7.61 \times 10^2\ L_\odot$, $\log T_e = 4.20$

M_r/M	R cm	L erg s^{-1}	T K	ϱ gm cm^{-3}	X_1	X_4	X_{12}	X_{16}	Mode
0.00	0.00	0.00	1.81×10^8	2.45×10^4	0.000	0.004	0.596	0.400	Conv.
0.03	1.29×10^9	3.38×10^{35}	1.43	1.69	0.000	0.004	0.596	0.400	Conv.
0.037	1.40	3.57	1.37	1.57	0.000	0.011	0.614	0.375	Rad.
0.05	1.60	3.74	1.27	1.35	0.000	0.020	0.634	0.346	
0.07	1.86	3.95	1.16	1.06	0.000	0.034	0.655	0.311	
0.10	2.33	4.43	1.04	5.56×10^3	0.000	1.000	7.6×10^{-5}	2.5×10^{-8}	
0.15	3.14	4.83	9.27×10^7	2.70	0.000	1.000	6.8×10^{-8}	3.7×10^{-13}	
0.168	3.50	5.60	9.02	1.96	0.002	0.998	5.5×10^{-9}		
0.173	3.59	1.16×10^{36}	8.94	1.77	0.022	0.978	2.2×10^{-9}		
0.20	4.24	2.27	7.86	1.09	0.066	0.934	1.7×10^{-12}		
0.25	5.59	2.52	6.25	4.62×10^2	0.155	0.845			
0.263	6.03	2.59	5.87	3.59	0.192	0.808			
0.30	7.58	2.79	4.87	1.72	0.317	0.683			
0.35	1.05×10^{10}	2.97	3.80	6.71×10^1	0.495	0.505			
0.40	1.41	3.04	3.00	3.13	0.627	0.373			
0.45	1.79	3.05	2.48	1.78	0.703	0.297			
0.50	2.24	3.04	2.08	1.07	0.750	0.250			
0.60	3.19	3.02	1.52	4.62×10^0	0.785	0.215			
0.70	4.22	3.00	1.15	2.20	0.793	0.207			
0.80	5.55	2.99	8.52×10^6	9.46×10^{-1}	0.798	0.202			
0.90	7.88	2.98	5.45	2.51	0.800	0.200			
0.95	9.85	2.97	3.90	8.90×10^{-2}	0.800	0.200			
1.00	1.22×10^{11}	2.97×10^{36}	1.57×10^4	5.04×10^{-10}	0.800	0.200			

TABLE IIIB

Characteristics of the model at the end of core helium-exhaustion
$t = 4.174 \times 10^8$ yr

M_r/M	ε_{pp} erg gm^{-1} s^{-1}	ε_{CN} erg gm^{-1} s^{-1}	$\varepsilon_{3\alpha}$ erg gm^{-1} s^{-1}	$\varepsilon_{12,\,4}$ erg gm^{-1} s^{-1}	ε_{ν} erg gm^{-1} s^{-1}	ε_{Total} erg gm^{-1} s^{-1}	$\varepsilon_{grav.}$ erg gm^{-1} s^{-1}
0.00			1.23×10^{2}	1.15×10^{4}	1.09×10^{2}	1.15×10^{4}	2.70×10^{2}
0.03			1.73×10^{-1}	1.17×10^{2}	1.87×10^{1}	9.80×10^{1}	2.09×10^{2}
0.037			1.06×10^{0}	1.46×10^{2}	1.31×10^{1}	1.34×10^{2}	1.89×10^{2}
0.05			4.88×10^{-1}	5.71×10^{1}	7.80×10^{0}	4.97×10^{1}	1.66×10^{2}
0.07			7.28×10^{-2}	1.32×10^{1}	3.86×10^{0}	9.34×10^{0}	1.40×10^{2}
0.10			8.75×10^{0}	2.40×10^{-3}	1.53×10^{0}	7.22×10^{0}	1.56×10^{2}
0.15			1.33×10^{-2}	7.69×10^{-8}	0.643	−0.630	1.15×10^{2}
0.168	2.44×10^{0}	8.52×10^{3}	2.02×10^{-3}	2.41×10^{-9}	0.526	8.51×10^{3}	1.75×10^{2}
0.173	1.67×10^{2}	4.20×10^{4}	1.02×10^{-3}		0.490	4.21×10^{4}	1.12×10^{2}
0.20	7.00×10^{2}	1.46×10^{1}	5.40×10^{-7}		0.098	7.15×10^{2}	1.91×10^{1}
0.25	9.91×10^{2}	2.81×10^{-6}			0.010	9.91×10^{2}	-1.08×10^{1}
0.263	1.01×10^{3}	2.75×10^{-8}				1.01×10^{3}	-1.73×10^{1}
0.30	8.46×10^{2}					8.46×10^{2}	-3.39×10^{1}
0.35	4.17×10^{2}					4.17×10^{2}	-4.89×10^{1}
0.40	1.54×10^{2}					1.54×10^{2}	-5.08×10^{1}
0.45	5.18×10^{1}					5.18×10^{1}	-4.98×10^{1}
0.50	1.34×10^{1}					1.34×10^{1}	-4.65×10^{1}
0.60	1.50×10^{0}					1.50×10^{0}	-3.67×10^{1}
0.70	2.21×10^{-1}					2.21×10^{-1}	-2.89×10^{1}
0.80	2.35×10^{-2}					2.35×10^{-2}	-2.43×10^{1}
0.90							-1.50×10^{1}
0.95							
1.00							

star, because of the smaller core size and higher luminosity of the H-He star. At the stage of maximum core energy production the contribution of the core to the total luminosity is smaller than 0.37. The luminosity of the hydrogen-burning shell is largely responsible for the total outflow of the energy.

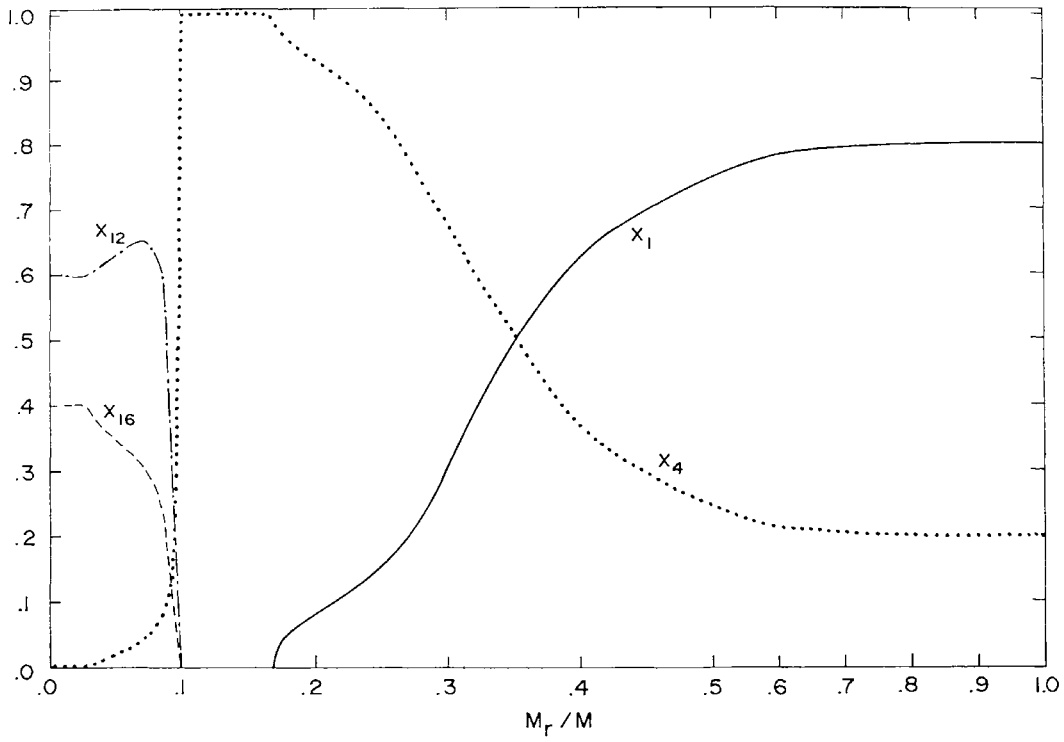

Fig. 8. The composition profile within the star for a model corresponding closely to the end of the core helium-exhaustion phase. The notations have their usual meanings.

If we define the core as that part of the star interior to the hydrogen-shell source, the mass of the core has increased from a value of 0.41 $M_\odot$ at the beginning of core helium ignition to a value of 0.50 $M_\odot$ near the end of core helium exhaustion. But it does not maintain a homogeneous composition.

In the hydrogen-burning shell, the energy generation rate has two maxima: the first at a mass fraction of 0.173 due to the CN-cycle reactions and the second at 0.263 due to the p-p chain reactions. The outer 15% of the star's mass still contains the initial composition of the stellar material.

Acknowledgement

The author is grateful to Dr A. G. W. Cameron and Dr J. Truran for the valuable discussions and to Dr R. Stothers for the helpful suggestion and assistance. This research has been supported in part by grants from the National Science Foundation and the National Aeronautics and Space Administration.

References

Austin, S. M., Trentelman, G. F., and Kashy, E.: 1971, *Astrophys. J.* **163**, L79.
Barkat, Z.: 1971, *Astrophys. J.* **163**, 433.
Beaudet, G., Petrosian, V., and Salpeter, E. E.: 1967, *Astrophys. J.* **150**, 979.
Biermann, P. and Kippenhahn, R.: 1971, *Astron. Astrophys* **16**, 32.
Böhm-Vitense, E.: 1958, *Z. Astrophys.* **46**, 108.
Cameron, A. G. W. and Truran, J. W.: 1971, *Astrophys. Space Sci.* **16**, 179.
Cauch, R., Spinka, T., Tombrello, T., and Weaver, T.: 1972, *Astrophys. J.* **172**, 395.
Ezer, D. and Cameron, A. G. W.: 1965, *Can. J. Phys.* **43**, 1497.
Ezer, D. and Cameron, A. G. W.: 1967, *Can. J. Phys.* **45**, 3429.
Ezer, D. and Cameron, A. G. W.: 1971a, *Astrophys. Space Sci.* **10**, 52.
Ezer, D. and Cameron, A. G. W.: 1971b, *Astrophys. Space Sci.* **14**, 399.
Fowler, W. A., Caughlan, G. R., and Zimmerman, B. A.: 1967, *Ann. Rev. Astron Astrophys.* **5**, 525.
Iben, I., Jr.: 1965a, *Astrophys. J.* **141**, 993.
Iben, I., Jr.: 1965b, *Astrophys. J.* **142**, 1147.
Paczynski, B.: 1970, *Acta Astron.* **20**, 47.
Parker, P. D.: 1968, *Phys. Rev.* **173**, 1021.
Reeves, H.: 1965, in L. H. Aller and D. B. McLaughlin (eds.), *Stars and Stellar Systems* **VIII**, University of Chicago Press, Chicago.
Salpeter, E. E.: 1954, *Australian J. Phys.* **7**, 373.